Mechanism of Aromatic Hydroxylation by an Activated Fe^{IV}=O Core in Tetrahydrobiopterin-Dependent Hydroxylases

Arianna Bassan,* Margareta R. A. Blomberg, and Per E. M. Siegbahn[a]

Abstract: The chemical pathways leading to the hydroxylated aromatic amino acids in phenylalanine and tryptophan hydroxylases have been investigated by means of hybrid density functional theory. In the catalytic core of these non-heme iron enzymes, dioxygen reacts with the pterin cofactor and is likely to be activated by forming an iron(IV)=O complex. The capability of this species to act as a hydroxylating intermediate has been explored. Depending on the protonation state of the ligands of the metal, two different mechanisms are found to be energetically possible for the hydroxylation of phenylalanine and tryptophan by the high-valent iron–oxo species. With a hydroxo ligand the two-electron oxidation of the aromatic ring passes through a radical, while an arenium cation is involved when a water replaces the hydroxide. After the attack of the activated oxygen on the substrate, it is also found that a 1,2-hydride shift (known as an NIH shift) generates a keto intermediate, which can decay to the true product through an intermolecular keto–enol tautomerization. The benzylic hydroxylation of 4-methylphenylalanine by the Fe^{IV}=O species has also been investigated according to the rebound mechanism. The computed energetics lead to the conclusion that Fe^{IV}=O is capable not only of aromatic hydroxylation, but also of benzylic hydroxylation.

Keywords: cofactors · density functional calculations · enzyme catalysis · hydroxylases · non-heme iron enzymes · O–O activation

Introduction

Aromatic amino acid hydroxylases are non-heme iron monooxygenases that use the organic cofactor tetrahydrobiopterin to catalyze the hydroxylation of phenylalanine, tyrosine, and tryptophan.[1–4] The hydroxylation reactions occurring in these three metalloenzymes are shown in Scheme 1. Phenylalanine hydroxylase (PAH) transforms phenylalanine to tyrosine, a reaction which initiates the catabolism of the amino acid phenylalanine. Tyrosine hydroxylase (TyrH) carries out the hydroxylation of tyrosine to L-DOPA, the rate-determining step in the biosynthesis of the neurotransmitters dopamine, adrenaline, and noradrenaline. Tryptophan hydroxylase (TrpH) converts tryptophan to 5-hydroxy-tryptophan, a precursor for the neurotransmitter serotonin (5-hydroxytryptamine).[1]

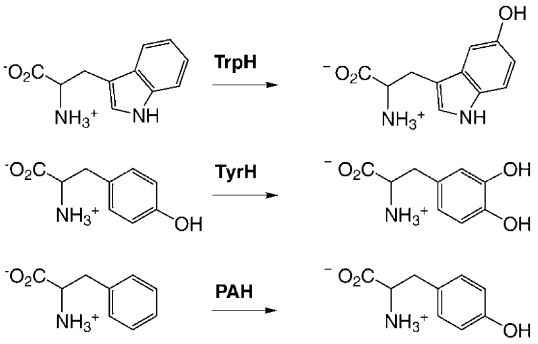

Scheme 1. Hydroxylation of aromatic amino acids catalyzed by phenylalanine hydroxylase (PAH), tyrosine hydroxylase (TyrH) and tryptophan hydroxylase (TrpH).

In the catalytic cores of these three enzymes, in which an iron atom anchored by the so called 2-His-1-carboxylate motif is hosted,[5, 6] molecular oxygen is consumed during the oxidation of the cofactor and the substrate. The cofactor (6*R*)-L-*erythro*-5,6,7,8-tetrahydrobiopterin (BH_4) undergoes a two-electron oxidation leading to pterin-4a-carbinolamine, while the aromatic amino acid is converted to the corresponding hydroxylated form.[1] The catalytic cycle requires a non-heme iron(II) complex and is initiated when all three substrates (i.e, the amino acid, the cofactor, and molecular oxygen) are bound in the active site of the metalloprotein. The resemblance of the chemical transformations occurring in PAH, TyrH, and TrpH together with the high sequential and structural homology of these three non-heme iron enzymes has led to the belief that catalysis in aromatic amino acid hydroxylases proceeds through similar mechanisms.[4] Despite a large number of experimental investigations, the reaction mechanism is still poorly understood and the exact role played by the metal center remains obscure.

[a] A. Bassan, Prof. M. R. A. Blomberg, Prof. P. E. M. Siegbahn
Department of Physics, Stockholm Center for Physics
Astronomy and Biotechnology, Stockholm University
106 91, Stockholm (Sweden)
Fax: (+46)8-55378600
E-mail: arianna@physto.se

 DOI: 10.1002/chem.200304768

The various experimental observations allow a simplistic scheme of the catalytic cycle to be drawn: substrate binding triggers oxygen activation and the subsequent formation of a hydroxylating intermediate, which is then responsible for hydroxylating the aromatic amino acid; the product dissociation concludes the cycle. The identity of the hydroxylating intermediate has not been revealed by any experiment yet. While for PAH and TyrH the formation of the hydroxylating intermediate appears to be rate limiting,[7–10] this is probably not the case for TrpH, for which kinetic isotope effects have been found when deuterium-substituted tryptophan is employed as substrate.[11] These experimental data, together with the evidence that the turnover numbers for PAH and TyrH are substantially higher than those of TrpH, have been related to the hydroxylation of the amino acid being slower than the formation of the hydroxylating intermediate in TrpH.

The crystal structures solved for PAH, TyrH, and TrpH hydroxylases with bound pterin indicate that the structural arrangement and orientation of the cofactor with respect to the iron complex are compatible with the formation of a peroxide species, the iron(II)-peroxy-BH_4 intermediate.[12–15] In the crystal structures of the three hydroxylases, the cofactor is in fact found positioned in the second coordination shell of the iron center at a distance that should allow the formation of the peroxide species. The pterin peroxide intermediate may then decompose into a high-valent iron–oxo species through O–O heterolysis. A mechanism which is shown in Scheme 2 for the specific case of PAH is then proposed, whereby the hydroxylation of the cofactor precedes the hydroxylation of the amino acid and leads to the formation of a high-valent iron–oxo intermediate, Fe^{IV}=O.[1, 4, 8, 16, 17] The subsequent hydroxylation of the aromatic substrate completes the enzyme catalysis. The involvement of an Fe^{IV}=O intermediate in the mechanism for the pterin-dependent hydroxylases is supported by experiments with synthetic non-heme iron catalysts; these have indicated that an Fe^{IV}=O is capable of aromatic hydroxylation.[18, 19] The mechanism depicted in Scheme 2 implies that the cofactor hydroxylation is independent of the substrate and the actual steps leading to the hydroxylated pterin might thus be commonly shared by the three hydroxylases.

The reaction mechanism which describes the amino acid hydroxylation should account for the experimental evidence that most of the tritium is retained in the products when [4-^{3}H]phenylalanine is hydroxylated by PAH (or TyrH) or when [5-^{3}H]tryptophan is hydroxylated by TrpH.[11, 20, 21] In the labeled products tritium is located in the site adjacent to the hydroxylated carbon. This migration is known as an NIH shift and it is observed also when *para*-substituted phenylalanines are used as substrates in PAH or TyrH.[3, 22] In this case the NIH shift is responsible for the formation of products containing the substituents (e.g., CH_3, Cl, Br) in the 3-position. Scheme 3 briefly summarizes the possible chemical routes that account for the NIH shift in aromatic

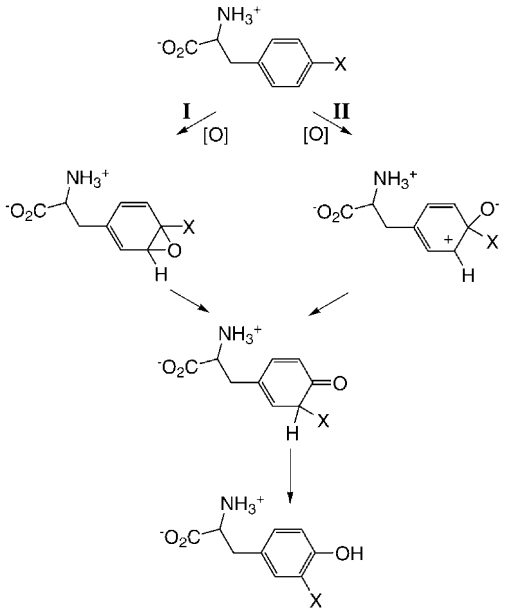

Scheme 3. Postulated mechanisms describing the aromatic hydroxylation in PAH; mechanism I involves an epoxide intermediate, while mechanism II involves an arenium cation.

hydroxylation.[1, 11, 23] One pathway (I) proceeds through an epoxide intermediate, which follows a concerted oxygen atom addition to the ring. The NIH shift then converts the epoxide to a ketone, and the subsequent enolization process gives the hydroxylated amino acid, in which the initial *para* substituent can be found *ortho* to the hydroxo group. The alternative route (II) instead involves an arenium cation. Subsequent NIH shift and enolization yield the final product. The isotope effects measured when deuterated phenylalanine reacts with TyrH support mechanism II and they also seem to contradict the involvement of an epoxide during substrate hydroxylation.[24]

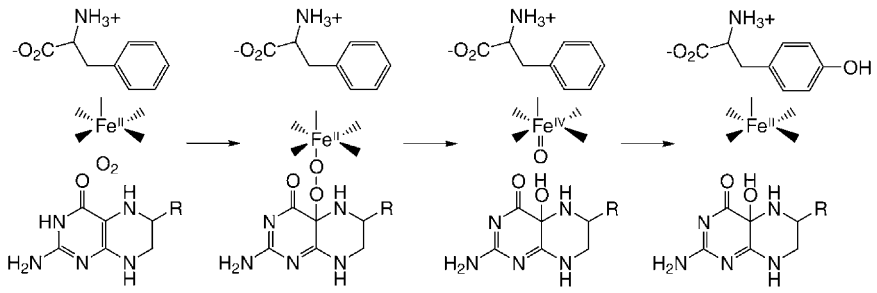

Scheme 2. Proposed mechanism describing the coupled hydroxylations of the aromatic substrate and of the pterin cofactor. The reaction involving phenylalanine is illustrated.

A recent hybrid density functional theory (DFT) investigation on tetrahydrobiopterin-dependent hydroxylases has shown the viability of a reaction mechanism involving an iron(II)–peroxy–BH_4 intermediate.[25]. It was also shown that the peroxide intermediate can subsequently undergo O–O bond heterolysis giving a high-valent iron–oxo species. The important question of whether

and how the activated non-heme Fe^{IV}=O core can carry out the two-electron oxidation of an arene still remains to be studied. In the present work the capability of the postulated iron–oxo intermediate to hydroxylate aromatic rings is thus probed by means of a hybrid DFT approach. Since experiments have highlighted significant kinetic differences between the hydroxylation processes occurring in PAH and TrpH,[11] the reaction mechanisms for these two hydroxylases have been addressed. Experiments have also shown that the hydroxylating intermediate in pterin-dependent hydroxylases is able to hydroxylate 4-methylphenylalanine giving 4-hydroxymethylphenylalanine together with the products of the aromatic hydroxylation.[22] In order to shed light on the oxidative capability of the postulated Fe^{IV}=O intermediate, the possible reaction pathway of benzylic hydroxylation has also been studied.

Computational Methods

The hydroxylation mechanism of the aromatic amino acids phenylalanine and tryptophan in pterin-dependent hydroxylases have been investigated by means of hybrid density functional theory (DFT) with the B3LYP functional,[26] which includes the Becke three-parameter exchange[27] and the Lee, Yang, and Parr correlation functionals.[28]

The two quantum chemical programs Gaussian 98[29] and Jaguar 4.1[30] were cooperatively employed in the present study. Initially the potential energy surfaces were probed by means of constrained optimizations to approximately locate transition states; afterward the computation of molecular Hessians (i.e., second derivatives with respect to the nuclear coordinates) of these structures was used to fully optimize the transition-state geometries. Molecular Hessians were calculated for the fully optimized structures of the reactants, intermediates, transition states, and products to evaluate the zero-point effects and the thermal corrections to the total energy, enthalpy, and Gibbs free energy. The thermochemical analysis, which uses standard expressions for an ideal gas in the canonical ensemble, treats the normal modes within the harmonic approximation. Evaluation of molecular Hessians for the transition state geometries was also needed to confirm that the structure is characterized by only one imaginary frequency corresponding to the normal mode associated to the reaction coordinate.

An effective core potential was used to describe iron.[31] In the geometry optimizations and in the Hessian evaluations all the other atoms were described by a standard double zeta basis set (labeled lacvp in Jaguar). The final B3LYP energies for the fully optimized structures were computed by using a large basis set with polarization functions on all atoms (labeled lacv3p** in Jaguar[30]). In the present work free energies include zero-point and thermal effects, evaluated for a temperature of 298.15 K.

The final energetics accounted for the actual environment in enzyme catalysis by means of a correction added to the gas-phase energy. The polarization effects induced by the protein environment were reproduced by modeling the solvent as a macroscopic continuum with a dielectric constant ε and the solute as placed in a cavity contained in this continuous medium. Specifically, the self-consistent reaction field as implemented in Jaguar was used to derive the solvent corrections by employing the lacvp basis set.[32, 33] A low dielectric constant ($\varepsilon = 4$) was chosen together with a probe radius of 1.4 Å. It was shown that the description of the protein environment as a continuum is sufficiently accurate to take into account the rather small long-range solvent effects.[34, 35]

The performance of the B3LYP functional was verified on the benchmark tests performed on a wide array of molecules including radicals, non-hydrogen systems, hydrocarbons, substituted hydrocarbons and inorganic hydrides (the G2-2 test set).[36, 37] These benchmarks showed that the B3LYP method has an average absolute deviation of 3.11 kcal mol^{-1}. When transition metals are involved, investigations on MR^+ complexes (R = H, CH_3, CH_2, OH) showed that the M–R bond energies computed with the B3LYP method have an error of 3.6–5.5 kcal mol^{-1}.[38, 39] It can be concluded that an error of about 3–5 kcal mol^{-1} is possibly affecting the energy profiles reported in the present investigation. However, such an accuracy should be enough to discriminate among different reaction mechanisms.[40]

Results and Discussion

The involvement of an Fe^{IV}=O intermediate during the coupled hydroxylations of the cofactor and the substrate in aromatic amino acid hydroxylases has often been invoked.[1, 4, 8, 16, 17] In the present study the capability of a high-valent iron–oxo moiety to carry out the two-electron oxidation of aromatic rings is probed. How the Fe^{IV}=O species can carry out benzylic hydroxylation is also examined. The first two subsections address the hydroxylation of phenylalanine with the aim of elucidating the reaction steps leading to tyrosine in PAH. While the first subsection deals with the two-electron oxidation of the phenyl ring to give a ketone, the second subsection describes the tautomerization reaction, which generates the actual hydroxylated substrate. In the third subsection the hydroxylation reaction in the 5-position of indole models the chemical transformations occurring in TrpH. The fourth subsection describes a possible reaction pathway leading to the benzylic hydroxylation of 4-methylphenylalanine. Before discussing the results for the aromatic and benzylic hydroxylations by Fe^{IV}=O, a brief summary of the previous DFT study, which demonstrated the feasibility of the high-valent iron–oxo species,[25] is given. An overview of the geometrical arrangement of the active site in the pterin-dependent hydroxylases is also presented in relation to the modeling approach adopted here.

The previous theoretical work showed that an iron(II)–peroxy–pterin intermediate can be obtained when dioxygen enters the first coordination shell of iron, forming a bridging bond between the cofactor and iron. The iron(II)–peroxy–pterin intermediate decomposes through O–O bond heterolysis to give 4a-carbinolamine and the hydroxylating intermediate HO–Fe^{IV}=O, whereby the hydroxide is generated by a proton transfer from a water ligand to the cofactor.

The model employed to investigate the cofactor hydroxylation was based on the crystal structures solved for the binary complex of PAH with pterin.[12, 13] The cofactor is found positioned in the second coordination shell of iron, which in turn coordinates two histidines (His285 and His290) and a monodentate glutamate (Glu330). The octahedral coordination of the metal is completed by three water ligands. An identical arrangement of the non-heme iron center was also found in the crystal structure recently solved for the binary complex TrpH-BH_4.[15] The crystal structure of the ternary complex of PAH with BH_4 and the substrate analogue 3-(2-thienyl)-L-alanine supports formation of an iron(II)–peroxy–pterin intermediate, with the cofactor still in the second coordination shell of the iron complex, but somewhat displaced toward the metal.[41] In the ternary complex the coordination environment of the metal still maintains the 2-His-1-carboxylate motif, but the glutamate (Glu330) is found coordinated in a bidentate fashion to iron with two Fe–O distances of 2.40 and 2.63 Å. The detection of the

density of only one water ligand in the first coordination shell means that at least one of the three water ligands in the PAH-BH_4 complex is lost when both the substrate and the cofactor are bound in the active site.[41] The change to a distorted square-pyramidal five-coordinate environment of the metal upon substrate binding agrees with CD and MCD spectroscopies,[42, 43] which indicated substantial perturbations in the ligand field when both the substrate and the cofactor are bound to the ferrous PAH. The five-coordinate metal might thus offer an open coordination site for oxygen activation.[17] EXAFS spectra measured for the PAH ternary complex with phenylalanine and the cofactor 6-methyltetrahydropterin still indicate a five-coordinate environment for iron, and they also support a monodentate glutamate.[44]

In the present theoretical study it is assumed that the Fe^{IV}=O intermediate coordinates a monodentate glutamate. Test calculations performed with an iron complex with a bidentate glutamate have shown that the actual arrangement of the carboxylate in the non-heme iron environment does not considerably affect the investigated chemistry. However, further studies on the effects of the bidentate glutamate on the O–O heterolytic process are required. The high-valent iron–oxo species depicted in Figure 1 is employed to probe

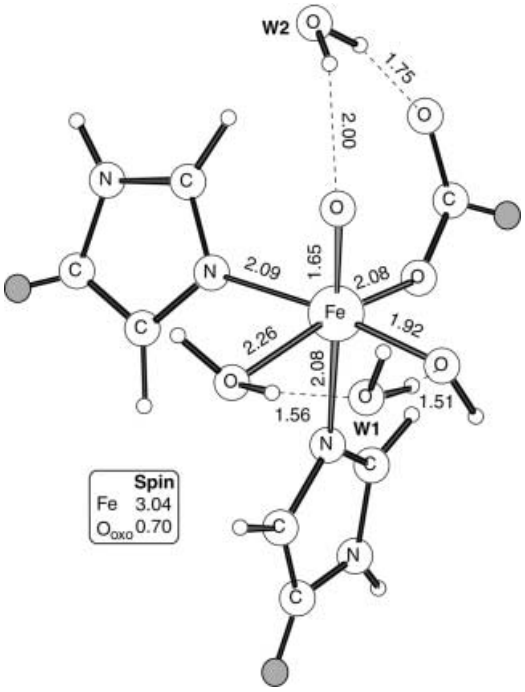

Figure 1. The HO–Fe^{IV}=O model employed to investigate aromatic and benzylic hydroxylations in pterin-dependent hydroxylases. Marked hydrogens corresponds to the connections with the protein backbone. The spin distribution and bond lengths [in Å] are shown.

whether and how an Fe^{IV}=O species can hydroxylate an aromatic ring as the second part of enzyme catalysis of pterin-dependent hydroxylases. The 2-His-1-carboxylate facial triad of the iron active site is modeled by two imidazole and one formate groups. A water molecule together with a hydroxo ligand complete the octahedral coordination of the iron–oxo species. The choice to model the hydroxylating intermediate as HO–Fe^{IV}=O is connected with the previous DFT investigation, whereby the hydroxo ligand was produced during the cofactor hydroxylation.[25] The structural arrangement of the Fe^{IV}=O complex employed here is thus based on the geometry of the metal complex generated after pterin hydroxylation. However, with respect to that model, two extra water molecules are also added in the second coordination shell of the metal (W1 and W2 in Figure 1). One water (W1) was found necessary to mimic the hydrogen-bonding network, which stabilizes the octahedral coordination of iron in the crystal structure. A second water molecule (W2) is placed so that is forms a hydrogen bond to the monodentate glutamate ligand. Test calculations with a model complex in which W2 was removed indicated that its presence does not affect the computed energies for the two-electron oxidation of the substrate. Nevertheless it was included in the system to better model the final steps of the reactions, which involve a proton transfer. It was proposed that before any enzymatic activity, Glu330 could promote the dissociation of one of the three water molecules ligated to iron in the PAH-BH_4 complex.[13, 25] Water W2 in the investigated system would consequently model the water dissociated from the octahedral non-heme complex.

It was previously found that the non-heme environment of iron creates a weak ligand field, explaining the computed quintet ground state for the HO–Fe^{IV}=O intermediate. The Fe=O double bond, analogous to the one in the O_2 molecule accounts for the short iron–oxygen distance (1.65 Å) and the peculiar spin distributions calculated for this complex (Figure 1).[25, 45] Two ferromagnetically coupled electrons occupy two degenerate π^* orbitals, leading to a localization of one electron on the metal and one on the oxo group; a total spin population of about three is located on the iron center. The triplet and the septet states, which are almost degenerate, lie quite close in energy to the quintet, higher by about 6 kcal mol^{-1}. Table 1 reports the spin distributions and the Fe–O bond lengths of these states. The electronic structure of the triplet differs from the one of the quintet in the coupling of the d electrons, but the geometry is still characterized by a short Fe–O bond length. On the other hand the bond between iron and the oxo oxygen atom cannot be described by an Fe=O double bond in the septet state, whereby an Fe–O bond length of 1.93 Å is obtained and a spin of 4.03 is computed on iron (this spin density on the metal corresponds to the ferric state of iron). Other states, such as the open shell M = 1 state (see Table 1) are much higher in energy than the quintet ground state.

Table 1. Spin distributions and Fe–O bond lengths of the high-valent iron–oxo species with different multiplicities (M = multiplicity). Spin densities on iron (Fe) and on the oxo group (O_{oxo}) are given. The energy difference (E) is also reported.

	M = 7	M = 5	M = 3	M = 1
spin (Fe)	4.03	3.04	1.21	0.67
spin (O_{oxo})	1.29	0.70	0.83	– 0.64
Fe–O [Å]	1.93	1.65	1.66	1.72
E [kcal mol^{-1}]	6.2	0.0	6.4	16.1

The energy profiles reported in the present work are derived from fully optimized structures, for which no coordinates were constrained to mimic the protein strain. However, some exploratory calculations were performed on a model system, whereby constraints were imposed on the two imidazole ligands and the monodentate glutamate in order to reproduce the actual rigidity of these ligands in the enzyme. When the positions of three hydrogen atoms (those marked in gray in Figure 1) were locked according to the X-ray crystal structure, the calculations showed that the added constraints perturb the energy profile of the two-electron oxidation of phenylalanine by less than 2 kcal mol^{-1}.

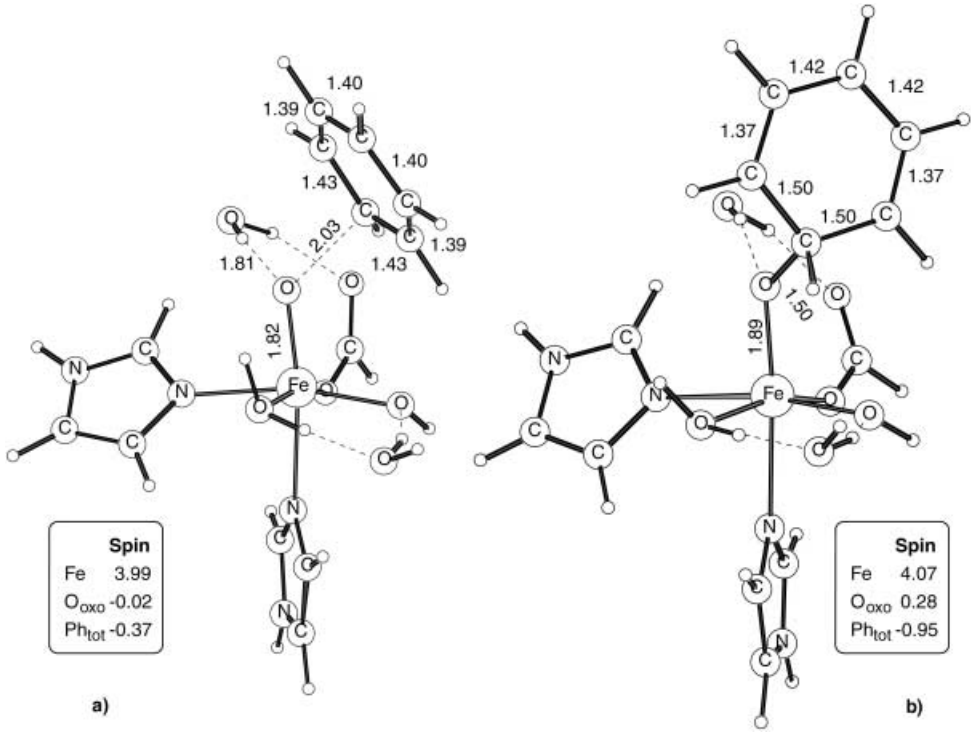

Figure 2. a) The transition state corresponding to the C–O bond formation in the PAH modeling. b) The radical (HO-Fe^{III}-O-Ph$^{\bullet}$) following the C–O bond formation in the PAH modeling. The computed spin densities on iron, on the oxo group (O_{oxo}), and the phenyl ring (Ph_{tot}) are shown. Bond lengths [in Å] are also shown.

The aromatic hydroxylation reaction of a model system with a water molecule instead of the hydroxo ligand has also been considered, and the results will be presented below and compared with those collected for HO–Fe^{IV}=O. The [H_2O–Fe^{IV}=O]$^+$ model mimics the enzyme catalysis if the OH ligand is protonated before substrate hydroxylation or if it is strongly hydrogen bonding; alternatively this model might reflect a different reaction pathway, whereby the O–O bond cleavage does not generate any hydroxide.

The two-electron oxidation of phenylalanine by Fe^{IV}=O: Hydroxylation of phenylalanine by HO–Fe^{IV}=O was investigated with the complex shown in Figure 1, in which benzene was also added in order to model phenylalanine. The initial location of the substrate with respect to the non-heme iron site was arbitrarily chosen, since the residues that anchor phenylalanine in the protein were not included in the modeling. It was found that the first step of benzene oxidation by the oxo–ferryl complex is the formation of a new C–O bond, via the transition state depicted in Figure 2a. The spin distribution reported in Figure 2a indicates that iron becomes reduced during the C–O bond formation. The spin density equal to 3.99 on the metal is typical for the high-spin ferric ion, which delocalizes the remaining spin associated with the five unpaired electrons on the ligands. The elongation of the Fe–O bond from 1.65 Å in the reactant to 1.82 Å in the transition state also reflects the reduction of the metal from iron(IV) to iron(III) during the ring oxidation. The process leads to the formation of a radical on the arene, for which a spin of -0.37 is computed at the transition state.

The transition state for the C–O bond formation decays to the intermediate shown in Figure 2b, whereby the unpaired electron localized in the phenyl ring (spin density is -0.95) is antiferromagnetically coupled to the five d electrons of the ferric ion (spin density is 4.07). It is worth noting that, in the proposed mechanism II of Scheme 3, the C–O bond formation leads to an arenium cation and a ferrous ion, while in the present model the first reaction step is associated with a one-electron oxidation of the ring, thus yielding ferric iron and a radical. The involvement of a radical in the catalysis of pterin-dependent hydroxylases resembles one of the proposed mechanisms for aromatic hydroxylation by the P450-dependent enzymes, whereby a radical is invoked.[23] The formation of a radical rather than an arenium cation is connected with the presence of the hydroxo ligand, since for the alternative model [H_2O–Fe^{IV}=O]$^+$, in which a water molecule is replacing the hydroxide, a carbocation was obtained after C–O bond formation. For that system, characterized by a total positive charge, the two-electron oxidation of benzene is accomplished during the C–O bond formation; this is not the case if the reactant is the HO–Fe^{IV}=O species. A detailed comparison between the energy profiles calculated for the two different models will be presented below.

The reaction coordinate along different potential-energy surfaces has also been analyzed leading to the conclusion that the C–O bond formation occurs along the quintet potential-energy surface. It is evident that the septet state of the HO-Fe^{III}-O-Ph$^{\bullet}$ species (a state whereby the unpaired electron on the ring is ferromagnetically coupled to the d electrons of iron) is degenerate with the corresponding quintet state of Figure 2b. It is therefore not surprising that the activation energy for the C–O bond formation along the septet surface is only a few kcal mol^{-1} higher in energy than the corresponding

one along the quintet state. The states (triplet or open shell singlet) of the HO-Fe^{III}-O-Ph$^{\cdot}$ species with one unpaired electron on the metal and one on the ring are about 15 kcal mol^{-1} higher in energy than the corresponding quintet ground state.

As shown in Figure 3, which reports the energy diagram for the two-electron oxidation of benzene by HO–Fe^{IV}=O leading to a ketone, the C–O bond formation requires

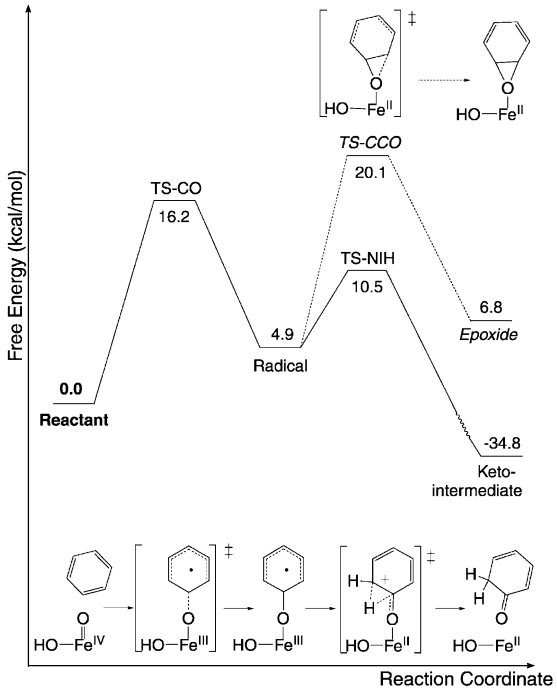

Figure 3. Computed energy diagram describing the two-electron oxidation of benzene by HO–Fe^{IV}=O.

an activation energy of 16.2 kcal mol^{-1} and is endergonic by 4.9 kcal mol^{-1}. The investigation of the subsequent chemical transformations reveals that the C–O bond formation is the slowest step in the hydroxylation process of benzene by the HO–Fe^{IV}=O species. The calculated energy barrier of 16.2 kcal mol^{-1} shows the viability of phenylalanine hydroxylation through the high-valent iron–oxo intermediate. This activation energy is very similar to the one previously obtained for the cofactor hydroxylation (16.6 kcal mol^{-1}).[25] The computed activation energies are in general agreement with experiments, which show that the rate-determining step in PAH catalysis does not involve attack of the amino acid substrate, but rather oxidation of the cofactor. Experiments have also indicated that when 6-methyl-5,6,7,8-tetrahydrobiopterin (6-MePH4) is used in place of BH_4 in PAH, hydroxylation of cofactor and hydroxylation of the amino acid occur with comparable rates.[3] Due to the similarity between BH_4 and 6-MePH4, this evidence suggests that the coupled hydroxylations of the cofactor and of the substrate should have activation energies that are not very different. The model system employed for the present theoretical investigation thus seems sufficient to reproduce the true energetics.

As mentioned above, hydroxylation of phenylalanine is found to start with a one-electron oxidation giving the HO-Fe^{III}-O-Ph$^{\cdot}$ intermediate. The two-electron oxidation is successfully completed during the following step, the NIH shift, which involves the transition state shown in Figure 4a. Since the calculated spin density of 3.77 located on iron typically corresponds to a high-spin ferrous ion, the two-electron oxidation of the aromatic ring is already accomplished at the transition state. The absence of any unpaired electron in the substrate confirms this observation. Furthermore, the computed total charge in the arene suggests that the transition state of Figure 4a can be interpreted as an arenium cation undergoing a 1,2-hydride shift. Due to the asymmetric environment, the NIH shift has been probed in both directions in the phenyl ring, but no significant difference appeared. The transition state of Figure 4a, which lies 10.5 kcal mol^{-1} higher in energy than the HO–Fe^{IV}=O reactant, decays to the keto intermediate of Figure 4b. The large exergonicity of 34.8 kcal mol^{-1} associated with this chemical step (Figure 3) makes the formation of the ketone irreversible. As Figure 4b shows, the product of the NIH shift is the oxidized substrate dissociated from the metal and located in the second coordination shell. It was found that the dissoci-

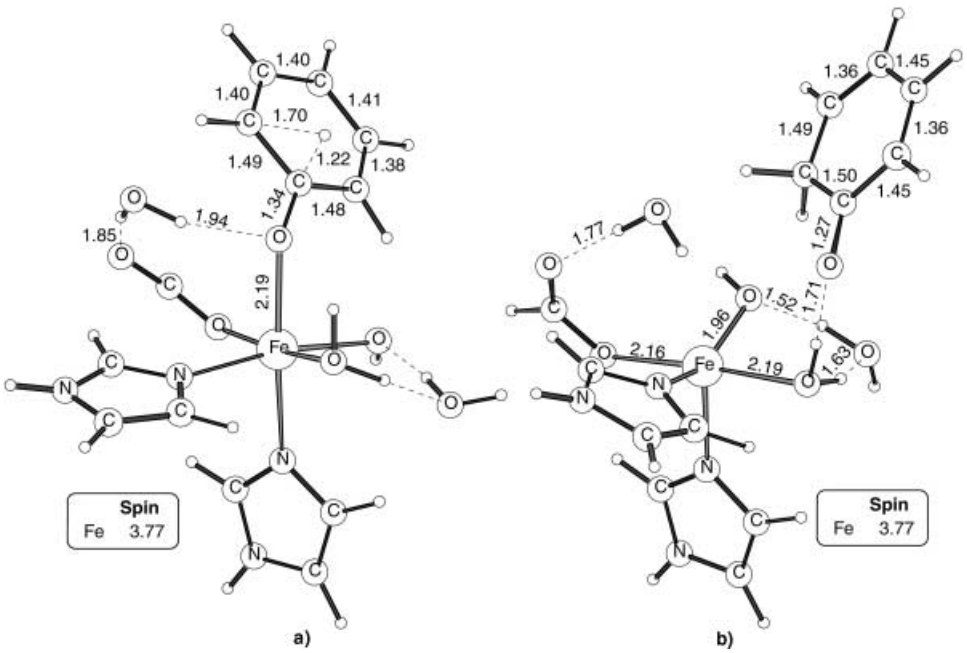

Figure 4. a) The transition state corresponding to the NIH shift in the PAH modeling. b) The keto intermediate generated by the two-electron oxidation of the aromatic ring in the PAH modeling. The computed spin densities on iron are shown. Bond lengths [in Å] are also shown.

ation of the ketone from the non-heme iron complex does not require any significant activation energy, since it is facilitated by a favorable hydrogen-bonding network created by the water molecules of the first and second coordination shell. The spin population in the iron center (3.77) reported in Figure 4b confirms the ferrous oxidation state, as already inferred from the spin distribution of the preceding transition state. At this point of catalysis, iron is back to the initial oxidation state, indicating that its redox catalytic activity has been completed. The enolization reaction, during which iron stays Fe^{II}, concludes phenylalanine hydroxylation. This step is described in the following subsection.

Since experiments have suggested that an epoxide might be involved in the hydroxylation reaction (Figure 3), this possibility has also been probed. A transition state corresponding to the simultaneous formation of two C–O bonds could not be found, but the calculations show that an epoxide can be generated from the radical of Figure 2b through the formation of a second C–O bond. This chemical transformation occurs with a high-energy barrier with respect to the reactant (20.1 kcal mol^{-1}) and, as in the case of the NIH shift, is accompanied by the reduction of the metal to iron(II) and the two-electron oxidation of the ring. The transition state and the subsequent product (i.e., the arene oxide) are shown in Figure 5 together with the corresponding spin distributions, which are indicative of ferrous ion. From the collected results, it can be concluded that, once the first C–O bond is formed, the reaction can continue through two different channels. As shown in Figure 3, an epoxide may be generated with an energy barrier of 15.2 kcal mol^{-1} with respect to the HO-Fe^{III}-O-Ph$^{\cdot}$ intermediate. However, a much smaller barrier (5.6 kcal mol^{-1}) is required for the NIH shift, which irreversibly leads to the ketone. The computed values for these two energy barriers show that the NIH shift is considerably favored over the epoxide formation. Calculations were also performed showing that the epoxide cannot undergo any NIH shift through a low-energy pathway. If the epoxide is formed, it can reversibly go back to the HO-Fe^{III}-O-Ph$^{\cdot}$ intermediate, from where the reaction could proceed toward the ketone. Although the transition state leading to the epoxide does not lie at a low energy, the computed barrier of 20.1 kcal mol^{-1} is not prohibitively high. It is thus concluded that the epoxide is not an obligatory intermediate, but it might still be energetically accessible.

The oxidation of benzene giving the keto intermediate has been investigated also for the slightly different model, whereby the hydroxide of the HO–Fe^{IV}=O species was substituted by a water molecule. The energy profile obtained with this alternative model is rather similar to the one reported in Figure 3. The main difference in terms of chemical mechanism is associated with the product of the first step, as already explained above. With the $[H_2O–Fe^{IV}=O]^+$/benzene model, the C–O bond formation leads to a ferrous complex and an arenium cation, which undergoes a zero-barrier NIH shift forming the ketone. Also for this system, the reaction was found to occur along the quintet potential-energy surface. A transition state for concerted oxygen-atom insertion leading to the epoxide was not located for this model either. Figure 6 describes a summary of the energy profile corresponding to benzene hydroxylation by $[H_2O–Fe^{IV}=O]^+$. A lower barrier (10.0 kcal mol^{-1}) is required for the initial C–O bond formation in the case of the $[H_2O–Fe^{IV}=O]^+$ model than the one obtained with HO–Fe^{IV}=O (16.2 kcal mol^{-1}). It is also evident that both approaches give a preference to the NIH shift over the epoxide formation. It is interesting to note that the main difference between the two models is related to the capability of the iron–oxo species to carry out the two-electron oxidation of the aromatic ring. In the HO–Fe^{IV}=O model, the HO-Fe^{III}-O-Ph$^{\cdot}$ intermediate is formed after the first attack of the oxo group on the ring, and the positive charge of the ferric ion is stabilized by the presence of two negatively charged ligands, the carboxylate and the hydroxo ligands. On the other hand, the $[H_2O–Fe^{IV}=O]^+$ model, with only one negative ligand (Glu330) carries out the two-electron redox process in one step. The different behavior of the two models is also reflected in the value of the two activation energies for the C–O bond formation, which implies an electron flow from the ring to the oxo group. It is clear that the additional negative ligand in the HO–Fe^{IV}=O makes the reduction of the metal from Fe^{IV} to Fe^{II} more difficult.

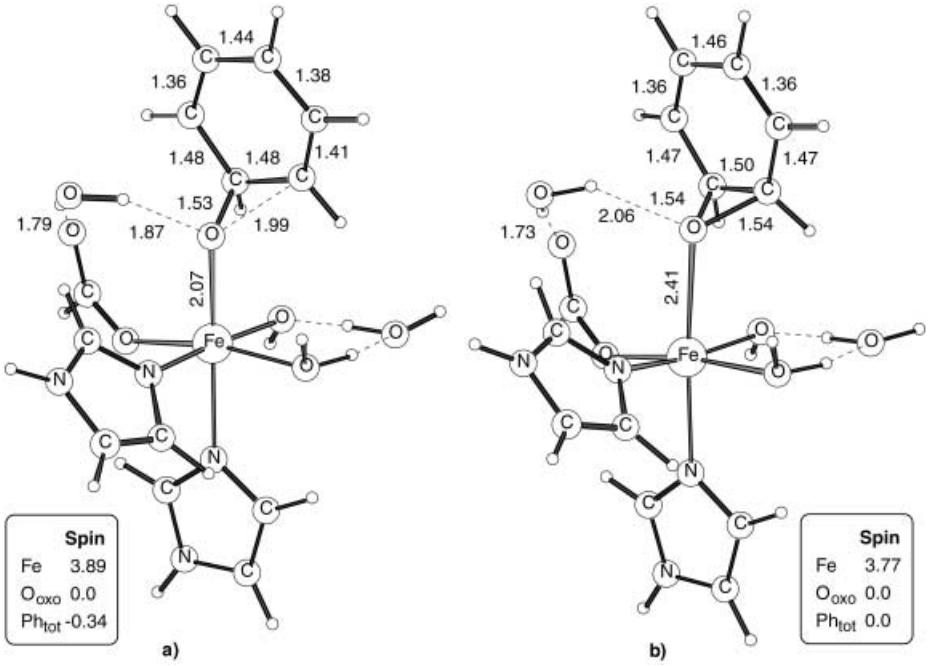

Figure 5. a) The transition state corresponding to the formation of a second C–O bond leading to an epoxide in the PAH modeling. b) The epoxide intermediate in the PAH modeling. The computed spin densities on iron, on the Fe-O-Ph oxygen (O_{oxo}), and the phenyl ring (Ph_{tot}) are shown. Bond lengths [in Å] are also shown.

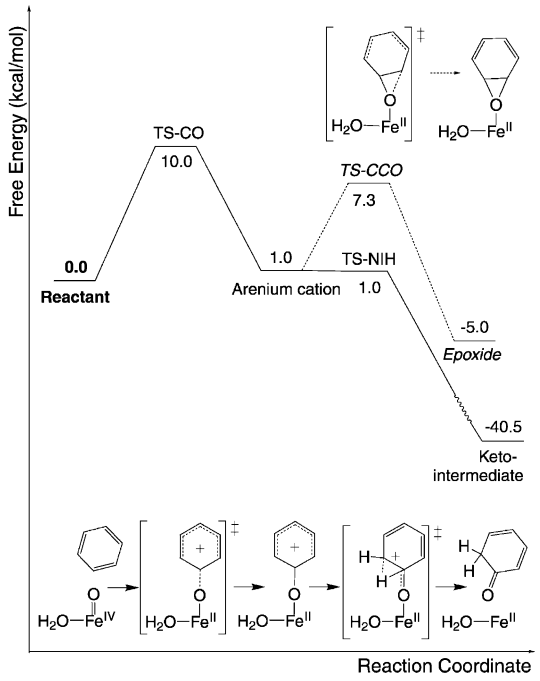

Figure 6. The energy profile for the two-electron oxidation of benzene by $[H_2O–Fe^{IV}=O]^+$.

The available experimental data and the rather similar energy profiles computed for the two models ($HO–Fe^{IV}=O$/benzene and $[H_2O–Fe^{IV}=O]^+$/benzene) do not allow any conclusion on which system properly reflects the actual chemical transformations occurring in PAH. However the two models may be regarded as two extremes of the actual mechanism describing the PAH catalysis. Therefore the computed energetics obtained in both cases demonstrate that the two-electron oxidation of phenylalanine can be accomplished by the high-valent iron–oxo species.

The keto-phenol tautomerization reaction: After the two-electron oxidation of benzene, the final product of aromatic hydroxylation is obtained through a tautomerization reaction yielding the phenol. Since an intramolecular enolization is found to require too high a barrier, the tautomerization process must be assisted by a suitable molecule, which acts as proton shuttle. It was chosen to probe if one of the water molecules in the second coordination shell of the metal complex (W2 of Figure 1) could participate in the intermolecular enolization leading to the final hydroxylated product, which is the phenol. Figure 7 highlights the geometrical details and the energy profile corresponding to the proton transfer assisted by W2 in the keto intermediate (Figure 4). The structure of the transition state and the normal mode with the imaginary frequency (i.e., the reaction coordinate) indicate that this transition state is mainly associated with the formation of a protonated water molecule, which is stabilized by the presence of the negative Glu, and which ultimately donates the proton to form phenol. The keto–enol tautomerization passing through the transition state of Figure 7 requires a barrier of 12.9 kcal mol^{-1} and is computed to be exergonic by 18.9 kcal mol^{-1} with respect to the keto intermediate of Figure 4b and by 53.7 kcal mol^{-1} with respect to the initial $Fe^{IV}=O$ reactant. During enolization, the water W2 is pulled toward the first coordination shell of iron, contributing to the restoration of the iron complex ready to restart the catalytic cycle.

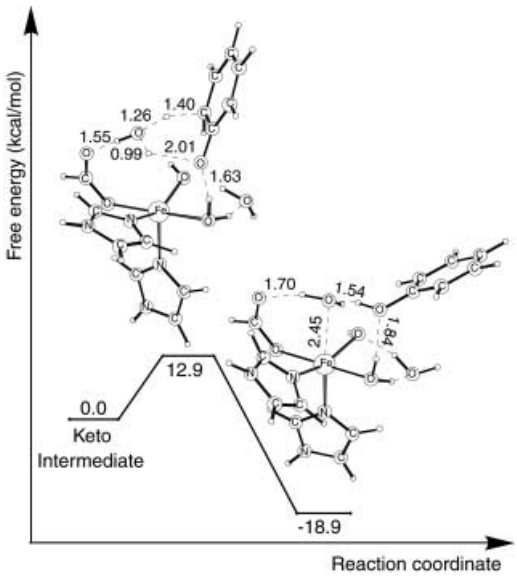

Figure 7. The geometrical details and the energy profile corresponding to the tautomerization reaction of benzene assisted by a second coordination shell water. Bond lengths [in Å] are shown.

The transition state reported in Figure 7 can be compared to the one obtained for the simpler model depicted in Figure 8, whereby the proton shuttle was investigated with a phenyl ring and a water molecule, removing the iron complex.

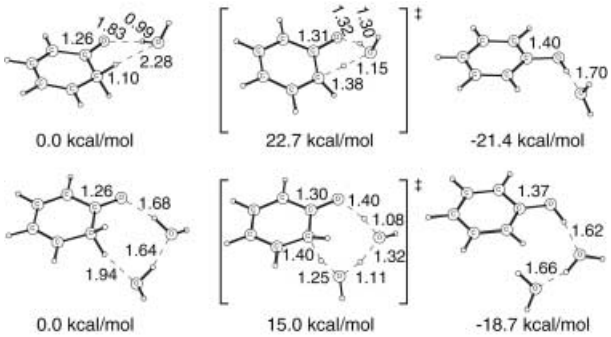

Figure 8. The geometrical details and the energy profile corresponding to the tautomerization reaction of benzene assisted by one and two water molecules. Bond lengths [in Å] are shown.

In this case the enolization requires an activation energy of 22.7 kcal mol^{-1} and is found to be exergonic by 21.4 kcal mol^{-1} with respect to the ketone. The computed barrier is rather high and indicates that a single water molecule is probably not sufficient to catalyze the enolization reaction. The catalysis carried out by two hydrogen bonding water molecules (Figure 8) considerably lowers the barrier down to 15.0 kcal mol^{-1}. From the energy values reported in Figure 8, it can be concluded that two hydrogen bonding water molecules present in the enzyme are able to catalyze the intermolecular enolization of the ketone. Alternatively, an arrangement such

as the one presented in Figure 7 still allows the tautomerization catalyzed by only one water.

The aromatic hydroxylation of tryptophan by Fe^{IV}=O: Catalysis in TrpH has been modeled with the HO−Fe^{IV}=O/indole system, similar to the corresponding modeling for PAH. The computed energy profile, which is summarized in Figure 9, highly resembles the one found for phenylalanine. The numbering used to refer to the different carbon atoms of indole is also highlighted in this figure.

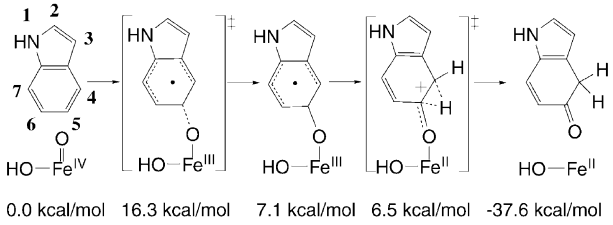

Figure 9. The energetics corresponding to the two-electron oxidation of indole by HO−Fe^{IV}=O.

Hydroxylation of tryptophan starts with the one-electron oxidation of the ring, leading to iron(III) and a radical in the substrate. The geometrical arrangement and the spin distribution of the transition state associated with the formation of the new C−O bond (Figure 10a) are very similar to the corresponding ones obtained for benzene, with iron evolving toward the ferric oxidation state (the computed spin density on iron is 3.98) and with a radical developing on the indole (the computed spin density on the indole is −0.40). Also the barrier for the one-electron oxidation of indole is found to be identical to that for benzene, 16.2 kcal mol^{-1} for the PAH model and 16.3 kcal mol^{-1} for the TrpH model. The C−O bond formation is found to be endergonic by 7.1 kcal mol^{-1} and reversibly yields a ferric intermediate, whereby one unpaired electron is delocalized in the arene and is antiferromagnetically coupled to the unpaired electrons of the metal. As already noted, the energy profile of the one-electron oxidation of benzene resembles very much that obtained for indole. This can be related to the similar stability of the two oxyarene radicals formed after Fe^{IV}=O reacts with indole or benzene.

Once the new C5−O bond has been formed after the one-electron oxidation of indole, a keto intermediate is obtained through the NIH shift, which, a priori, could occur either toward C4 or toward C6. Both directions were investigated and were found to occur without any barrier with respect to the ferric intermediate. It is worth mentioning that the transition states for the two NIH shifts were indeed located (Figure 10b reports the structure and the spin distribution for one of the two transition states), but a rather big basis correction of the order of −5 kcal mol^{-1} (i.e., the lacv3p** correction added to the lacvp energies as described in the computational details) together with the zero point and thermal corrections of about −2 kcal mol^{-1} canceled out the activation energy. As found for the benzene case, the NIH shift is associated with the reduction of the metal from Fe^{III} to Fe^{II}, showing that the current chemical process can be viewed as a reduction of iron immediately followed by a 1,2-hydride shift of an arenium cation. The hydrogen shift leads to a ketone, which, as in the benzene case, can dissociate from the iron complex with an almost zero barrier. The redox catalytic activity of the metal is completed when the keto intermediate is obtained and iron is back to the ferrous oxidation state. The energy profile reported in Figure 9 shows that the NIH shift is an irreversible process occurring with an exergonicity of 37.6 kcal mol^{-1} with respect to the initial HO−Fe^{IV}=O species.

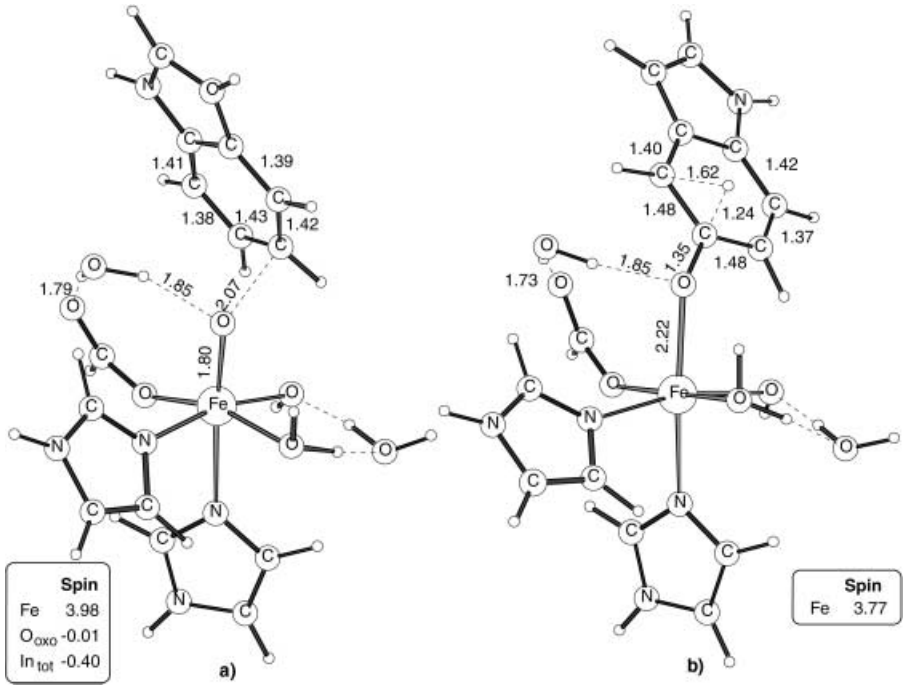

Figure 10. The structures for the transition state associated with the C−O bond formation (a) and the transition state associated with the NIH shift toward C4 (b) in the TrpH modeling. The computed spin densities on iron, on the oxo group (O_{oxo}), and in the aromatic ring (In_{tot}) are shown. Bond lengths [in Å] are also shown.

The final tautomerization reaction of the ketone yielding 5-HO-indole has been explored with two different models as done for the PAH modeling. The proton transfer catalyzed by the water molecule, hydrogen bonding to Glu330 (W2) in the keto intermediate, was compared to the one catalyzed by two hydrogen-bonding water molecules, but without the iron complex. An intramolecular enolization, or alternatively an intermolecular proton transfer assisted by only one water, were estimated to require too high activation energies. Table 2 summarizes the energy profiles of the tautomerization reaction for the two investigated systems, the metal/indole

Table 2. The energy profiles [kcal mol^{-1}] describing the enolization reaction yielding 5-HO-indole (see text). The barrier for the proton transfer catalyzed by the water molecule hydrogen bonding to Glu300 (W2) in the ferric keto intermediate (metal/indole model) is compared to that obtained with a simpler model including only indole and two hydrogen-bonding waters (two waters/indole model).

	Ketone	Transition State	5-HO-Indole
metal/indole model	0.0	18.0	– 17.4
two waters/indole model	0.0	15.9	– 18.4

model and the two waters/indole model. The latter involves a barrier of 15.9 kcal mol^{-1} and the former have a barrier of 18.0 kcal mol^{-1}. From Table 2, it can also be noted that an almost identical exergonicity has been evaluated for the proton shuttle in the two different models.

At this stage the main features of the mechanism for tryptophan hydroxylation can be summarized. The two-electron oxidation of the aromatic substrate starts with the formation of a new C–O bond, which requires a barrier (16.3 kcal mol^{-1}) very similar to the one previously computed for the hydroxylation of the pterin cofactor (16.6 kcal mol^{-1}). Afterward, the reaction proceeds through an NIH shift, leading to a ketone. The probabilities for the NIH shift to occur in one or in the other direction are found to be identical. The subsequent tautomerization of the ketone requires the catalytic activity of two hydrogen-bonding water molecules or of one water molecule assisted by a negatively charged metal ligand. In both cases, the activation energy corresponding to the enolization process is comparable to the C–O bond formation.

A rather similar picture is obtained from the investigation of indole hydroxylation for the $[H_2O–Fe^{IV}=O]^+$ model. The structural arrangements of the transition states corresponding to the latter approach very much resemble the ones obtained for the HO–Fe^{IV}=O/indole model and they are therefore not reported here. Figure 11 summarizes the energy profile

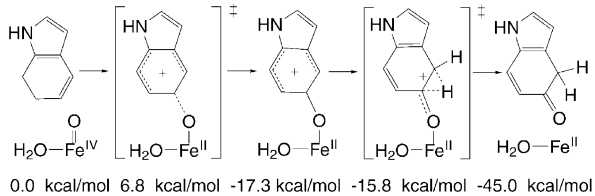

Figure 11. he energetics corresponding to the two-electron oxidation of indole by $[H_2O–Fe^{IV}=O]^+$.

provided by the study of the hydroxylation reaction with $[H_2O–Fe^{IV}=O]^+$. As for the corresponding benzene case illustrated above, the first C–O bond formation leads to an arenium cation, implying a two-electron oxidation of the aromatic substrate. However, this step is found to be irreversible, in contrast to the corresponding reversible reaction obtained for benzene and also in contrast to the reversible reaction obtained for the C–O bond formation in the HO–Fe^{IV}=O/indole model. This difference can be ascribed to the capability of indole to stabilize a positive charge. With a water molecule instead of the hydroxo ligand in the Fe^{IV}=O complex, the formation of the C–O bond is easier, requiring an activation energy of only 6.8 kcal mol^{-1} instead of 16.3 kcal mol^{-1}. The arenium cation is converted to a ketone by the NIH shift, whereby the activation energy (with respect to the arenium cation) is still very small, although not zero as in the previous HO–Fe^{IV}=O/indole model. The NIH shift is again found to occur in both directions, since the computed barriers toward C4 or C6 are small and very similar, 1.5 and 3.6 kcal mol^{-1} (with respect to the arenium cation) respectively.

The calculated energy profiles for the HO–Fe^{IV}=O/indole model give comparable activation energies for the hydroxylation of tryptophan and the activation of dioxygen, 16.3 and 16.6 kcal mol^{-1}, respectively. Considering a normal error of the B3LYP method of a few kcal mol^{-1}, this result does not contradict the experimental interpretation that substrate hydroxylation is likely to be rate-determining in TrpH. The quite small error could also be related to an additional structural parameter, which has been excluded from the present modeling. For example, experiments suggest that the nitrogen of the indole could play an important role for the appropriate positioning of the amino acid through an essential hydrogen bonding.[46] Experiments indicate an inverse secondary kinetic isotope effect of 0.93 with 5-^{2}H-tryptophan, but no inverse isotope effect with 4-^{2}H-tryptophan (the measured isotope effect was in this case 1.03).[11] It was thus suggested that the isotope effect could be ascribed to the C–O bond formation during the substrate hydroxylation, which in turn has to involve a higher barrier than the one of the cofactor hydroxylation. By using transition-state theory, an inverse isotope effect of 0.92 has indeed been computed for the formation of the radical with deuterium in the 5-position (0.92 for the formation of the indole cation in the $[H_2O–Fe^{IV}=O]^+$ as well). When deuterium was substituted in the 4-position, an isotope effect of 1.10 was found.

If the results for the HO–Fe^{IV}=O/indole model, as described above, can be considered as in general agreement with experiments, this can not be said about results for the $[H_2O–Fe^{IV}=O]^+$/indole model. In this case, the calculated barrier for substrate hydroxylation is only 6.8 kcal mol^{-1}. This value is much too low relative to the dioxygen activation of 16.3 kcal mol^{-1} to be considered in agreement with the experimental interpretation that substrate hydroxylation is rate-limiting. The conclusion from the results of these different models is therefore that the model with an hydroxo group on iron models the actual situation best, at least for tryptophan hydroxylase but probably also for phenylalanine hydroxylase.

As mentioned above, the NIH shift is experimentally found to occur only from C5 to C4.[11] The present results with both models show that the barriers for the NIH shifts are very small. In the case of the $[H_2O–Fe^{IV}=O]^+$/indole a slight preference for the shift toward C4 is actually computed, but for the HO–Fe^{IV}=O/indole the NIH shift was found to occur without any barrier in both directions. In this situation, with very small or no barriers, the present type of model studies are not sufficient for determining steric preferences. It appears most likely that the preference for the NIH shift toward C4 is determined by details of the dynamics, which are not well described by transition-state theory but require a much more

sophisticated dynamical treatment. This is beyond the scope of the present study.

The benzylic hydroxylation of 4-methylphenylalanine by Fe^{IV}=O: In order to analyze the capability of pterin-dependent hydroxylases to carry out benzylic hydroxylation,[22, 47] methyl hydroxylation of toluene by HO–Fe^{IV}=O has been investigated. The results are summarized in Figure 12, in

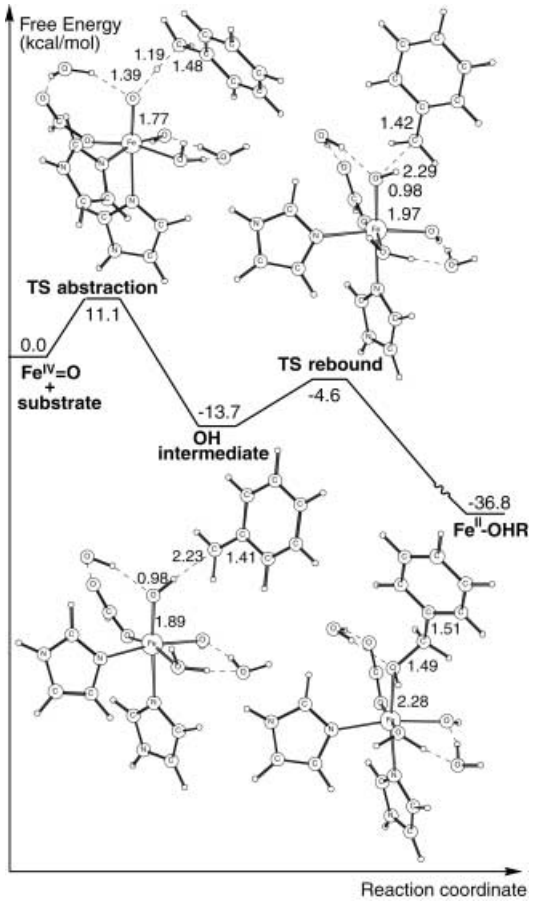

Figure 12. Energy diagram and corresponding structures for the rebound mechanism of toluene and HO–Fe^{IV}=O. Bond lengths [in Å] are shown.

which the computed energy diagram is presented together with the structures of the transition states and intermediates.

Oxidation of toluene by the high-valent iron–oxo species (in the quintet ground state) starts with hydrogen atom abstraction from the methyl group, in agreement with the widely accepted mechanism describing alkane hydroxylation in cytochrome P450.[23] The process involves a barrier of 11.1 kcal mol^{-1}, which includes a considerable correction of about -5 kcal mol^{-1} due to zero-point effects. This correction, which significantly lowers the activation energy, is typical for hydrogen-atom abstraction; a similar value was found, for example, in methane monooxygenase (MMO).[48] The spin distribution (Table 3) associated with the transition states (TS abstraction and TS rebound of Figure 12) and with the intermediates (OH intermediate and Fe^{II}-OHR of Figure 12) is indicative of the redox processes occurring during the rebound mechanism. The computed spin of the TS-abstraction transition state (spin density of 3.88 on iron and -0.27 localized on the methyl carbon) reflects the reduction of iron toward Fe^{III} and the development of a radical on the substrate during the hydrogen atom abstraction. The following intermediate (OH intermediate of Figure 12) indeed contains a ferric ion and an unpaired electron delocalized on the substrate. As already explained above, the spin density of 4.12 found on iron of the OH intermediate is typical of the high-spin iron(III). The unpaired electron of the radical substrate is antiferromagnetically coupled to the five d electrons of the metal and it generates a spin of -0.72 on the methyl carbon and a delocalized spin of -0.26 in the aromatic ring. It is interesting to note that the hydrogen-atom abstraction from toluene is exergonic by 13.7 kcal mol^{-1}, as opposed to the corresponding intermediate following the hydrogen-atom abstraction from methane by an oxo–ferryl species in P450.[49, 50] The computed exergonicity of this step is connected with the stability of the radical intermediate with the electron partially delocalized in the aromatic ring. The rebound mechanism with the non-heme iron complex is also different from the one in P450, whereby there is an additional radical (on the porphyrin) in the reactant and in the corresponding OH intermediate.

Table 3. The computed spin distribution for the reactant (Fe^{IV}=O), transition states (TS-abstraction, TS-rebound), and intermediates (OH intermediate, Fe^{II}-OHR) in the rebound mechanism (see text and Figure 12). Spin densities on iron (Fe), on the oxo group (O_{oxo}), on the phenyl ring (Ph), and on the methyl carbon (C) are given.

	Fe^{IV}=O	TS abstraction	OH intermediate	TS rebound	Fe^{II}-OHR
spin (Fe)	3.04	3.88	4.12	4.01	3.77
spin (O_{oxo})	0.70	0	0.32	0.29	0
spin (Ph)	0	0	-0.26	-0.17	0
spin (C)	0	-0.27	-0.72	-0.51	0

According to the rebound mechanism proposed for alkane hydroxylation in P450, the next step in the benzylic hydroxylation is the radical rebound, which involves the TS-rebound transition state lying at 9.1 kcal mol^{-1} with respect to the previous intermediate. From a thermodynamic point of view, the rebound step occurs with a large exergonicity (-36.8 kcal mol^{-1}) and it leads to the final hydroxylated product (Fe^{II}–OHR). It is important to note that during the rebound step, iron is further reduced to Fe^{II} and is then ready to carry out another catalytic cycle. The computed activation energies for the hydrogen-atom abstraction and the radical rebound indicates that the first step is rate-limiting for the benzylic hydroxylation by the Fe^{IV}=O species. The barrier for substrate hydroxylation is considerably lower than that associated with the cofactor hydroxylation.

By examining different potential-energy surfaces, corresponding to different spin states, it was found that the rebound mechanism occurs along the quintet potential-energy surface. It is interesting to remember that the septet and triplet states of the iron(IV)–oxo species are energetically quite similar to the quintet state (see Table 1). However, the activation energy for the hydrogen-atom abstraction along the triplet potential-energy surface, is about 10 kcal mol^{-1} higher than the corresponding quintet transition state; also for the OH intermediate, the triplet state lies about 8 kcal mol^{-1} higher in energy

than the corresponding quintet structure. Because of these energy differences and since the ground state of the product is a quintet, the triplet potential-energy surface has not been further investigated. On the other hand, it is clear that the septet state of the OH intermediate (the unpaired electrons on the metal and on the substrate are ferromagnetically coupled) is degenerate with the quintet state, whose spin distribution is shown Table 3. Therefore it is not surprising that also the septet TS-abstraction transition state is almost degenerate with the corresponding quintet structure. The rebound step, however, must still involve the quintet potential-energy surface, since the septet product is very high in energy.

The rebound mechanism, which can explain how the benzylic hydroxylation occurs, is feasible because of the relatively weak methyl C–H bond in toluene. A similar hydrogen-atom abstraction for benzene would not be possible. The computed benzylic C–H bond strength is 86 kcal mol^{-1} as compared to the 109 kcal mol^{-1} found for benzene.

Conclusions

In the present study, quantum chemical calculations at the B3LYP level of theory shows the capability of an activated Fe^{IV}=O core to hydroxylate phenylalanine and tryptophan during the second part of the catalytic cycle of tetrahydrobiopterin-dependent hydroxylases.

Previous theoretical work has shown that an iron(IV)–oxo hydroxylating intermediate can be generated during cofactor hydroxylation, which involves O–O heterolysis and a proton transfer from one of the waters ligated to the iron complex.[25] Based on those findings, a model with a hydroxo group coordinated to the metal center (HO–Fe^{IV}=O) was employed to probe the reaction mechanism of aromatic hydroxylation. Another model ([H_2O–Fe^{IV}=O]$^+$) with a water ligand in place of the hydroxide was also explored in order to mimic other possible reaction pathways. For both amino acids and for both models the slow step in the two-electron oxidation of the amino acid is the attack of the activated Fe^{IV}=O core on the substrate with the subsequent formation of a new C–O bond. The chemical transformations are found to occur along the quintet potential-energy surface, which is also the ground state for Fe^{IV}=O.

In the [H_2O–Fe^{IV}=O]$^+$ model, the C–O bond formation is associated with two-electron oxidation of the aromatic amino acid, consequently generating an arenium cation as an intermediate. This reaction step involves activation energies for phenylalanine and tryptophan that are much lower than that associated with dioxygen activation. In agreement with experiments, which indicated a migration of the hydrogen atom from the hydroxylated site to the adjacent one, it was found that the arenium cation undergoes a 1,2-hydride shift leading to a keto intermediate. With respect to the arenium cation, the NIH shift requires very low activation energies, almost zero for phenylalanine, a couple of kcal mol^{-1} for tryptophan.

Higher activation energies for the C–O bond formation are found for the HO–Fe^{IV}=O species, the other investigated model. In this case the iron–oxo species attacks phenylalanine or tryptophan with a barrier of about 16 kcal mol^{-1}, a value that is almost identical to the energy barrier previously found for dioxygen activation. When a hydroxo group coordinates the metal, the C–O bond formation implies a one-electron oxidation of the substrate, yielding a ferric ion and a radical delocalized on the substrate. The two-electron oxidation of the amino acid is completed in the next chemical step, when iron becomes Fe^{II} and simultaneously a 1,2-hydride shift leads to the keto intermediate. The calculated activation energies show that for this model the rates for the two coupled hydroxylations of the cofactor and the substrate are comparable.

The findings acquired from the present quantum chemical calculations agree with the various experimental data collected for phenylalanine hydroxylase. The computed barriers for the hydroxylation of tryptophan is perhaps a bit too low with respect to the information given by experiments. Hence, a structural lack in the model for TrpH can possibly be invoked. Nevertheless when the two models (HO–Fe^{IV}=O and [H_2O–Fe^{IV}=O]$^+$) for PAH and TrpH are regarded as two possible extremes of the true enzyme catalysis, an important conclusion can be drawn from the computed energetics, and this is the feasibility of aromatic hydroxylation by a high-valent iron–oxo species. This conclusion is additionally supported by other calculations performed on benzylic hydroxylation of 4-methylphenylalanine by Fe^{IV}=O. The calculated energetics for the hydrogen-atom abstraction and for the subsequent rebound step indicate that the high-valent iron–oxo species can carry out methyl hydroxylation, as indeed is observed experimentally in the aromatic amino acid hydroxylases.

Acknowledgements

We thank Prof. Lawrence Que, Jr. (University of Minnesota, Minneapolis) for helpful discussions on non-heme iron enzymes. We are also grateful to Prof. Paul F. Fitzpatrick (Texas A&M University, Texas) for valuable comments. We gratefully acknowledge the National Supercomputer Center (Sweden) for generous grants of computer time at the SGI3800.

[1] T. J. Kappock, J. P. Caradonna, *Chem. Rev.* **1996**, *96*, 2659–2756.
[2] T. Flatmark, R. C. Stevens, *Chem. Rev.* **1999**, *99*, 2137–2160.
[3] P. F. Fitzpatrick, *Annu. Rev. Biochem.* **1999**, *68*, 355–381.
[4] P. Nordlund, in *Handbook of Metalloproteins* (Eds: I. Bertini, A. Sigel, H. Sigel), Marcel Dekker, New York, **2001**, pp. 461–570.
[5] E. L. Hegg, L. Que, Jr., *Eur. J. Biochem.* **1997**, *250*, 625–629.
[6] L. Que, Jr., *Nat. Struct. Biol.* **2000**, *7*, 182–184.
[7] W. A. Francisco, G. Tian, P. F. Fitzpatrick, J. P. Klinman, *J. Am. Chem. Soc.* **1998**, *120*, 4057–4062.
[8] J. P. Klinman, *J. Biol. Inorg. Chem.* **2001**, *6*, 1–13.
[9] P. F. Fitzpatrick, *Biochemistry* **1991**, *30*, 6386–6391.
[10] P. F. Fitzpatrick, *Biochemistry* **1991**, *30*, 3658–3662.
[11] R. G. Moran, A. Derecskei-Kovacs, P. J. Hillas, P. F. Fitzpatrick, *J. Am. Chem. Soc.* **2000**, *122*, 4535–4541.
[12] H. Erlandsen, E. Bjørgo, T. Flatmark, R. C. Stevens, *Biochemistry* **2000**, *39*, 2208–2217.
[13] O. A. Andersen, T. Flatmark, E. Hough, *J. Mol. Biol.* **2001**, *314*, 279–291.

[14] K. E. Goodwill, C. Sabatier, R. C. Stevens, *Biochemistry* **1998**, *37*, 13437 – 13445.
[15] L. Wang, H. Erlandsen, J. Haavik, P. M. Knappskog, R. C. Stevens, *Biochemistry* **2002**, *41*, 12569 – 12574.
[16] T. D. H. Bugg, *Curr. Opin. Chem. Biol.* **2001**, *5*, 550 – 555.
[17] E. I. Solomon, T. C. Brunold, M. I. Davis, J. N. Kemsley, S.-K. Lee, N. Lehnert, F. Neese, A. J. Skulan, Y.-S. Yang, J. Zhou, *Chem. Rev.* **2000**, *100*, 235 – 349.
[18] S. J. Lange, H. Miyake, L. Que, Jr., *J. Am. Chem. Soc.* **1999**, *121*, 6330 – 6331.
[19] M. P. Jensen, S. J. Lange, M. P. Mehn, E. L. Que, L. Que, Jr., *J. Am. Chem. Soc.* **2003**, *125*, 2113 – 2128.
[20] J. Renson, J. Daly, H. Weissbach, B. Witkop, S. Udenfriend, *Biochem. Biophys. Res. Commun.* **1966**, *25*, 504 – 513.
[21] G. Guroff, J. W. Daly, J. Renson, B. Witkop, S. Udenfriend, *Science* **1967**, *157*, 1524 – 1530.
[22] P. J. Hillas, P. F. Fitzpatrick, *Biochemistry* **1996**, *35*, 6970 – 6975.
[23] M. Sono, M. P. Roach, E. D. Coulter, J. H. Dawson, *Chem. Rev.* **1996**, *96*, 2841 – 2887.
[24] P. F. Fitzpatrick, *J. Am. Chem. Soc.* **1994**, *116*, 1133 – 1134.
[25] A. Bassan, M. R. A. Blomberg, P. E. M. Siegbahn, *Chem. Eur. J.* **2003**, *9*, 106 – 115.
[26] P. J. Stevens, F. J. Devlin, C. F. Chablowski, M. J. Frisch, *J. Phys. Chem.* **1994**, *98*, 11623 – 11627.
[27] A. D. J. Becke, *Chem. Phys.* **1993**, *98*, 5648 – 5652; A. D. J. Becke, *Chem. Phys.* **1992**, *96*, 2155 – 2160; A. D. J. Becke, *Chem. Phys.* **1992**, *97*, 9173 – 9177.
[28] C. Lee, W. Yang, R. G. Parr, *Phys. Rev.* **1988**, *B37*, 785 – 789.
[29] Gaussian 98, M. J. Frisch, G. W. Trucks, H. B. Schlegel, G. E. Scuseria, M. A. Robb, J. R. Cheeseman, V. G. Zakrzewski, J. A. Montgomery, Jr., R. E. Stratmann, J. C. Burant, S. Dapprich, J. M. Millam, A. D. Daniels, K. N. Kudin, M. C. Strain, O. Farkas, J. Tomasi, V. Barone, M. Cossi, R. Cammi, B. Mennucci, C. Pomelli, C. Adamo, S. Clifford, J. Ochterski, G. A. Petersson, P. Y. Ayala, Q. Cui, K. Morokuma, D. K. Malick, A. D. Rabuck, K. Raghavachari, J. B. Foresman, J. Cioslowski, J. V. Ortiz, A. G. Baboul, B. B. Stefanov, G. Liu, A. Liashenko, P. Piskorz, I. Komaromi, R. Gomperts, R. L. Martin, D. J. Fox, T. Keith, M. A. Al-Laham, C. Y. Peng, A. Nanayakkara, C. Gonzalez, M. Challacombe, P. M. W. Gill, B. Johnson, W. Chen, M. W. Wong, J. L. Andres, C. Gonzalez, M. Head-Gordon, E. S. Replogle, and J. A. Pople, Gaussian, Inc., Pittsburgh PA, **1998**.
[30] JAGUAR 4.1: Schrödinger, Inc., Portland, Oregon, **2000**; see: G. Vacek, J. K. Perry, J.-M. Langlois, *Chem. Phys. Lett.* **1999**, *310*, 189 – 194.
[31] P. J. Hay, W. R. Wadt, *J. Chem. Phys.* **1985**, *82*, 299 – 310.
[32] D. J. Tannor, B. Marten, R. Murphy, R. A. Friesner, D. Sitkoff, A. Nicholls, M. Ringnalda, W. A. Goddard III, B. Honig, *J. Am. Chem. Soc.* **1994**, *116*, 11875 – 11882.
[33] B. Marten, K. Kim, C. Cortis, R. A. Friesner, R. B. Murphy, M. Ringnalda, D. Sitkoff, B. Honig, *J. Phys. Chem.* **1996**, *100*, 11775 – 11788.
[34] P. E. M. Siegbahn, *J. Comput. Chem.* **2001**, *22*, 1634 – 1645.
[35] P. E. M. Siegbahn, M. R. A. Blomberg, *Chem. Rev.* **2000**, *100*, 421 – 437.
[36] L. A. Curtiss, K. Raghavachari, G. W. Tucks, J. A. Pople, *J. Chem. Phys.* **1991**, *94*, 7221 – 7230.
[37] L. A. Curtiss, K. Raghavachari, P. C. Redfern, J. A. Pople, *J. Chem. Phys.* **1997**, *106*, 1063 – 1079.
[38] M. R. A. Blomberg, P. E. M. Siegbahn, M. Svensson, *J. Chem. Phys.* **1996**, *104*, 9546 – 9554.
[39] A. Ricca, C. W. Bauschlicher, Jr., *J. Phys. Chem. A* **1997**, 8949 – 8955.
[40] M. R. A. Blomberg, P. E. M. Siegbahn, in *Transition State Modeling for Catalysis* (Eds.: D. G. Truhlar and K. Morokuma), American Chemical Society, Washington DC, **1999**, pp. 49 – 60.
[41] O. A. Andersen, T. Flatmark, E. Hough, *J. Mol. Biol.* **2002**, *320*, 1095 – 1108.
[42] K. E. Loeb, T. E. Westre, T. J. Kappock, N. Miti, E. Glasfeld, J. P. Caradonna, B. Hedman, K. O. Hodgson, E. I. Solomon, *J. Am. Chem. Soc.* **1997**, *119*, 1901 – 1915.
[43] J. N. Kemsley, N. Miti, K. L. Zaleski, J. P. Caradonna, E. I. Solomon, *J. Am. Chem. Soc.* **1999**, *121*, 1528 – 1536.
[44] E. C. Wasinger, N. Miti, B. Hedman, J. Caradonna, E. I. Solomon, K. O. Hodgson, *Biochemistry* **2002**, *41*, 6211 – 6217.
[45] K. Yoshizawa, Y. Shiota, T. Yamabe, *J. Am. Chem. Soc.* **1998**, *120*, 564 – 572.
[46] G. R. Moran, R. S. Phillips, P. F. Fitzpatrick, *Biochemistry* **1999**, *38*, 16283 – 16289.
[47] P. F. Fitzpatrick, *J. Am. Chem. Soc.* **2002**, *124*, 4202 – 4203.
[48] P. E. M. Siegbahn, R. H. Crabtree *J. Am. Chem. Soc.* **1997**, *119*, 3103 – 3113.
[49] F. Ogliaro, N. Harris, S. Cohen, M. Filatov, S. P. de Visser, S. Shaik, *J. Am. Chem. Soc.* **2000**, *122*, 8977 – 8989.
[50] K. Yoshizawa, T. Kamachi, Y. Shiota, *J. Am. Chem. Soc.* **2001**, *123*, 9806 – 9816.

Received: January 27, 2003 [F4768]

